HHS Public Access

Author manuscript

J Control Release. Author manuscript; available in PMC 2018 November 28.

Published in final edited form as:

J Control Release. 2017 November 28; 266: 248–255. doi:10.1016/j.jconrel.2017.09.043.

Radiation-enhanced delivery of systemically administered amphiphilic-CpG oligodeoxynucleotide

Oliver K. Appelbe[a], **Kelly D. Moynihan**[b], **Amy Flor**[a], **Nick Rymut**[a], **Darrell J. Irvine**[c], and **Stephen J. Kron**[a,*]

[a][1] Ludwig Center for Metastasis Research, The University of Chicago, 5758 South Maryland Avenue, MC 9006, Chicago, IL 60637, United States of America [2] Department of Molecular Genetics and Cellular Biology, The University of Chicago, 929 East 57th Street, GCIS W519, Chicago, IL 60637, United States of America

[b][1] Department of Biological Engineering, Massachusetts Institute of Technology, Cambridge, Massachusetts 02139, USA [2] Koch Institute for Integrative Cancer Research, Massachusetts Institute of Technology, Cambridge, Massachusetts 02139, USA

[c][1] Department of Materials Science and Engineering, Massachusetts Institute of Technology, Cambridge, Massachusetts 02139, USA [2] Department of Biological Engineering, Massachusetts Institute of Technology, Cambridge, Massachusetts 02139, USA [3] Koch Institute for Integrative Cancer Research, Massachusetts Institute of Technology, Cambridge, Massachusetts 02139, USA [4] Ragon Institute of Massachusetts General Hospital, Massachusetts Institute of Technology, and Harvard, Cambridge, Massachusetts 02139, USA [5] Howard Hughes Medical Institute, Chevy Chase, Maryland 20815, USA

Abstract

Along with vaccines and checkpoint blockade, immune adjuvants may have an important role in tumor immunotherapy. Oligodeoxynucleotides containing unmethylated cytidyl guanosyl dinucleotide motifs (CpG ODN) are TLR9 ligands with attractive immunostimulatory properties, but intratumoral administration has been required to induce an effective anti-tumor immune response. Following on recent studies with radiation-targeted delivery of nanoparticles, we examined enhanced tumor-specific delivery of amphiphile-CpG, an albumin-binding analog of

[*]**Corresponding author:** Stephen J. Kron, The University of Chicago, GCIS W522A, 929 East 57th Street, Chicago, IL 60637, phone - (773) 834-0250, fax - (773) 702-3611, skron@uchicago.edu.

Author contributions

O.K.A., K.D.M., D.J.I., and S.J.K. initiated the project. O.K.A. led experimental design, data acquisition and analysis, and manuscript preparation. K.D.M. designed and prepared all CpG formulations and assisted with manuscript preparation. A.F. contributed to experimental design, data acquisition and analysis, and manuscript preparation. N.R. aided in data acquisition. D.J.I. and S.J.K. participated in experimental design, data analysis, and manuscript preparation.

Conflict of interest statement

The authors declare no potential conflicts of interest.

Supplementary data

Supplementary material.

CpG ODN, following systemic administration 3 days after tumor irradiation. The combination of radiation and CpG displayed superior tumor control over either treatment alone. Intravital imaging of fluorescently labeled amphiphilic-CpG revealed increased accumulation in irradiated tumors along with decreased off-target accumulation in visceral organs. Within 48 hrs after amphiphile-CpG administration, immune activation could be detected by increased Granzyme B and Interferon gamma activity in the tumor as well as in circulating monocytes and activated $CD8^+$ T cells. Using radiotherapy to enhance the targeting of CpG to tumors may help advance this once promising therapy to clinical relevance.

Graphical abstract

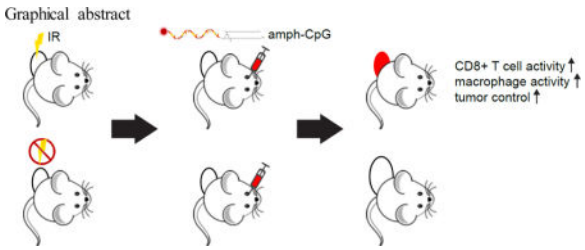

Keywords

CpG oligodeoxynucleotides; ionizing radiation; immune adjuvant; enhanced permeability and retention; cancer therapeutic efficacy

Introduction

While checkpoint blockade antibodies are responsible for much of the current excitement in immuno-oncology, on their own, these agents stimulate objective tumor regression in only a fraction of patients, and treatment can be accompanied by problematic toxicities. A challenge is to increase efficacy without similarly enhancing adverse effects. Studies combining checkpoint blockade with vaccines, adjuvants and conventional genotoxic agents such as radiation therapy are each under active investigation.

Small, oligodeoxynucleotides rich in unmethylated cytidyl guanosyl dinucleotides (CpG ODNs) have demonstrated promise as immune adjuvants in cancer immunotherapy in both preclinical and clinical studies. CpG ODNs serve as synthetic ligands that mimic bacterial infection and activate the pathogen-associated molecular pattern (PAMP) receptor Toll-like receptor 9 (TLR9) [1–3]. TLR9 is an endosome membrane-bound DNA sensor expressed primarily by B lymphocytes and plasmacytoid dendritic cells (pDCs) in humans, as well as by macrophages and myeloid dendritic cells (mDCs) in mice [1, 4]. Upon binding CpG-ODN, TLR9 activates a MYD88/IRF7/NF-κB dependent pathway [5, 6], resulting in production of proinflammatory cytokines and Type I interferons. Prominent cytokines include interleukin-1 (IL-1), IL-6, IL-18, and tumor necrosis factor alpha (TNFα) and a T-helper cell 1-biased (interferon gamma (IFNγ), and IL-12) immune milieu [7–9]. Thereby, CpG promotes dendritic cell maturation and antigen presentation along with secondary activation of a natural killer (NK) and T lymphocyte-mediated anti-tumor immune response

[7, 8, 10–14]. Depletion of $CD8^+$ T cells and NK cells abrogates CpG ODN's therapeutic effect [15, 16], reinforcing their roles as effectors of the immune response.

For CpG ODN to serve as an effective adjuvant and induce anti-tumor immunity, the activated innate immune cells must be able to present tumor antigens. Where CpG ODN can be dosed by intra- or peri-tumoral injection, immune-mediated tumor rejection can be observed [15, 17, 18]. Recently, we reported an amphiphilic form of CpG (amph-CpG) formed by conjugation of an albumin-binding diacyl lipid to the 5′ terminus of CpG ODN [19]. Amph-CpG displayed favorable lymph-node targeting properties when dosed by subcutaneous injection. Leveraging albumin's role as a carrier for fatty acids and other hydrophobic molecules in the body [20], the 5′ diacyl lipid can bind endogenous serum albumin to facilitate amph-CpG transport and accumulation in draining lymph nodes. Compared to unconjugated CpG ODN, amph-CpG displayed 30-fold increased T cell priming, enhanced therapeutic efficacy, and reduced systemic toxicity [19].

Although systemic administration of CpG ODN has shown efficacy in some studies [21–23], untargeted immunostimulation may have limited impact on anti-tumor immunity while CpG ODN accumulation in the liver and kidney may induce problematic toxicities [24]. A common strategy to obtain preferential delivery to tumors is to take advantage of the Enhanced Permeability and Retention (EPR) effect [25, 26], whereby circulating macromolecules and nanoparticles leak through endothelial gaps in the disordered tumor vasculature. Toward exploiting the EPR effect, systemic treatment with CpG ODN has been examined after liposomal encapsulation [27], polymer trapping [28], or conjugation to nanoparticles [29] but has yet to be translated to the clinic.

Conventional, external beam radiotherapy remains the most common treatment for cancer, though benefits have long remained modest at best. Much of the recent interest in radiotherapy has focused on two areas, high-dose, image-guided radiation delivery and strategies to enhance synergy between radiation and immunotherapy. Recently, we observed that a single dose of X-irradiation is sufficient to increase tumor microvascular permeability, leading to higher accumulation of systemically administered macromolecular agents and increased therapeutic effects over delivery by the EPR effect alone [30]. Going farther back, extravasation of serum albumin has long been noted to increase following irradiation [31, 32]. This raised the question whether delivery of albumin-tethered drugs might similarly be enhanced after tumor irradiation.

In this study, we used a mouse tumor model to examine whether the radiation-enhanced delivery effect might improve targeting of systemically administered, albumin-binding amph-CpG. Enhanced tumor accumulation after radiotherapy corresponded with significantly improved tumor control relative to amph-CpG treatment on its own. A benefit of enhanced tumor delivery appeared to be decreased accumulation off-target in the liver and kidneys. Combination treatment increased activated $CD8^+$ T lymphocytes and monocyte/macrophages both in circulation and in tumors. This surge in immune activity is likely responsible for the improved tumor growth control and could potentially lead to the elimination of metastases or prevention of recurrence.

Materials and Methods

Study design

Minimum sample size was calculated a priori using a power value of 0.80. Identification of outliers was performed using the ROUT method in Prism software. Data collection was discontinued when any dimension of a tumor exceeded 1 cm.

This research was undertaken to assess the effect of X-irradiation on delivery of systemically administered amph-CpG to transplanted tumors in mice. For tumor growth studies, treatment was initiated when tumors reached a volume of 25–50 mm^3. Animals were then assigned to treatment groups so that the mean tumor volume for each group was approximately equal. The mice were then treated with X-irradiation, injected with amphiphile-CpG 3 days later, and examined by intravital imaging as detailed below. Cages contained mice from multiple treatment groups and researchers did not sort animals by treatment group when collecting data.

Amphiphile-CpG oligodeoxynucleotide

Solid phase DNA synthesis and 5′ amphiphile conjugations were carried out as previously described using an ABI 394 synthesizer [19]. The CpG ODN sequence used was murine oligodeoxynucleotide class B sequence 1826 with two guanine spacers: 5′ diacyl lipid -*G*G*T*C*C*A*T*G*A*C*G*T*T*C*C*T*G*A*C*G*T*T- 3′ 3′-fluorophore-labeled oligonucleotides were synthesized on TAMRA or ROX long chain alkylamine controlled pore glass (lcaa CPG 500Å, ChemGenes) and cleaved and deprotected in t-butylamine/water (1:3) for 6 h at 60 °C. All oligonucleotides were purified using RP-HPLC and quantified using UV-Vis spectrometry as previously described [19].

Syngeneic tumor model

Six-week-old female BALB/c mice were purchased from Harlan Laboratories (Madison, WI, USA). TUBO murine mammary carcinoma cells, derived from BALB-neuT transgenic mice [33] were cultured in RPMI 1640 growth medium supplemented with 1 U/mL penicillin and 1 μg/mL streptomycin, then resuspended in sterile 1× DPBS at a concentration of 1×10^7 cells/mL for injection of 100 μL/mouse. 1×10^6 TUBO cells were injected subcutaneously into the hindlimb of mice to induce tumor growth and tumor volume was measured biweekly using calipers and calculated by the formula, $V = l \times w \times (h/2)$. Amphiphile-CpG (100 μg per animal, from [19]) was administered via retro-orbital injection in a volume of 100 μL. Animal studies were performed under ACUP# 72354 approved by the University of Chicago Institutional Animal Care and Use Committee.

Irradiation

An X-RAD 225Cx small animal irradiator (Precision X-Ray Inc., N. Bradford, CT, USA) was used to plan and deliver X-ray irradiation in a two-step process involving computed tomography [34] imaging followed by image-guided delivery of a precise treatment dose. The X-ray source was used for both imaging (1.0 mm focal spot) and treatment (5.5 mm focal spot). The subject was immobilized using isoflurane anesthesia and secured on the irradiator stage using surgical tape. Treatment planning began using the X-RAD 225C

software and involved two sequential CT images taken through a 2.0 mm Al filter including an initial scout image (40 kVp, 0.5 mA, 0.3 mm isotropic voxels), followed by a more detailed full scan (40 kVp, 2.5 mA, 0.1 mm isotropic voxels). DICOM files of the detailed CT scan were exported into a treatment planning application written in MATLAB (The MathWorks Inc., Natick, MA, USA) for selection of the treatment isocenter, planning of an irradiation protocol, and evaluation of the selected treatment fields. Irradiation protocols were designed with fields from two opposing directions, each delivering half the desired total dose. The software also calculated the 3D shift of the animal support stage required to position the chosen target at the radiation isocenter for treatment. Radiotherapy was performed following import of the treatment protocol into the XRAD 225C software, which automated delivery of the planned fields. Treatments were performed at 225 kVp, 13 mA and 0.3 mm Cu filter, with a 1.5 cm diameter lead collimator providing a dose rate of ~2.5 Gy/min. The irradiator output was calibrated according to the American Association of Physicists in Medicine Task Group 61 protocol [35] using a Farmer type chamber. Doses ranging from 5 to 10 Gy were used in this study with total treatment time lasting up to 15 min, including set-up.

Fluorescence imaging

To examine fluorescence in tissues *ex vivo*, the Xenogen IVIS 200 (Caliper Life Sciences, Hopkinton, MA, USA) was used at 1 d, 2 d, and 14 d after amphiphilic-CpG injection to quantitatively measure fluorescent probe permeation and retention in differentially treated tumors. Dissected tumors, as well as other tissues such as liver, spleen, heart, kidney, and lung, were imaged for amphiphile-CpG fluorescence. Intestinal CpG retention was not examined due to autofluorescence from ingested chow [36]. The radiant efficiency, a relative measure of photon emission from the tissue (photons/sec/cm^2/sr), was measured in a standardized region of interest (ROI) with variables such as exposure time, binning, and f/stop also standardized.

Flow cytometric analysis of leukocyte phenotype and activation

Peripheral whole blood samples were collected from the retro-orbital sinus with a capillary tube, centrifuged and the cell pellets frozen. Samples were thawed on ice in 1.0 mL of RPMI culture medium (Invitrogen, Carlsbad, CA, U.S.A.) for 10 min, centrifuged for 5 min at 500 *x g*, and vigorously resuspended in 2.0 mL of 1X red blood cell lysis buffer (Biolegend, San Diego, CA, U.S.A.). After 5 min at 24 °C, 3.0 mL of DPBS was added, samples were centrifuged 5 min at 500 *x g* and resuspended in 2.0 mL DPBS. Cell density was determined using a handheld cell counting device (Scepter, Millipore, Darmstadt, Germany). Then, 0.5 × 10^6 cells were centrifuged and leukocyte pellets were resuspended in 100 μL of blocking buffer consisting of 1% BSA + 5% normal goat serum (Jackson ImmunoResearch, West Grove, PA, U.S.A.) + 10 μg/mL Fc receptor blocking reagent (TruStain FCx, Biolegend) in 1X DPBS. Leukocytes were blocked for 20 min on ice with moderate vortexing at 10 min.

For leukocyte phenotyping, a cocktail of fluorophore-conjugated primary antibodies was added to samples, including anti-CD8 (clone 2.43, APC conjugate, 0.25 μg, Invitrogen), anti-CD19 (clone 6D5, PE conjugate, 0.25 μg, Biolegend), and anti-CD49b (clone DX5, Alexa Fluor 488 conjugate, 0.25 μg, Biolegend). Antibodies were added directly to cells in

blocking buffer and samples were stained for 30 minutes at 4°C in the dark with slow rotation. Samples were washed once in 1.0 mL of ice-cold wash buffer consisting of 1% BSA in 1X DPBS. A cellular viability/ROS stain (Calcein Violet 450 AM, eBioscience, San Diego, CA, U.S.A.) was then added to cells at 1 μM in 500 μL of 1% BSA-DPBS for 15 minutes on ice prior to flow cytometric data acquisition and analysis.

Flow cytometric data acquisition was carried out using a BD Fortessa instrument equipped with 4 lasers (405, 488, 561, and 640 nm) and appropriate fluorescent detectors. FACSDiva software was used to set up data acquisition parameters. Multispectral data for 50,000 viable cells were acquired per sample. Fluorophore spectral overlap was confirmed to be negligible using single-stained samples. Flow cytometric data analysis was performed using FlowJo software (TreeStar). Dead cells and doublets were excluded from analysis. Single cell events were identified by a conventional forward scatter gating approach (FSC-A vs FSC-H). Lymphocyte and monocyte subpopulations of leukocytes were established by scatter gating (FSC vs. SSC). Each population of cells was then evaluated for percentage of cells exhibiting positivity for each leukocyte marker ($CD8^+$ cytotoxic T cells, $CD19^+$ B cells, and $CD49b^+$ NK cells. For evaluation of leukocyte activation, the percentage of cells exhibiting a ROS-HI intensity signal provided by the Calcein Violet probe was determined using a standardized gating approach for each population of interest. Mean percentage of ROS-HI $CD8^+$ T cells and monocytes for n = 3 mice per treatment group was determined, as well as the standard deviation across mice in each treatment group. These data were then used for statistical analysis as described below.

Immunohistochemistry

Tumors and spleens were dissected from mice immediately following sacrifice and were fixed in 10% formalin. Tissue processing and embedding were performed by the Human Tissue Resource Center at the University of Chicago. Antibodies for Granzyme B (Abcam, Cambridge, MA, USA, ab4059, 1:600), F4/80 (Abcam, ab111101, 1:2000), and Interferon-γ (Novus Biologicals, Littleton, CO, USA, NBP-19761, 1:8000) were used for IHC of tissue sections. For IHC, 5 μm sections were treated by deparaffinization and serial rehydration. Antigen retrieval was performed with 10 mM sodium citrate buffer, pH 6.0 (or 10 mM Tris, 1 mM EDTA buffer, pH 9.0 for F4/80 staining) in a tissue steamer for 40 min at 96°C. Endogenous peroxidase activity was quenched with 1% H_2O_2 in methanol for 20 min. Blocking was with 2.5% normal horse serum for 20 min at 4°C. Primary antibodies were then applied on tissue sections overnight at 4°C in a humidity chamber. Following PBS washes, antibody binding was detected with ImmPRESS HRP polymer anti-rabbit IgG and ImmPACT DAB peroxidase substrate (Vector Laboratories, Burlingame, CA, USA). Tissue sections were briefly immersed in hematoxylin for counterstaining, quickly dehydrated, mounted using Poly-Mount (Polysciences Inc., Warrington, PA, USA), and cover glassed.

Imaging was performed at the University of Chicago Integrated Light Microscopy Facility. Images were captured with a Zeiss Axioplan upright microscope with a Zeiss Axiocam color CCD camera (Carl Zeiss Microscopy, Thornwood, NY, USA) run by the QCapture suite (QImaging, Surry, BC, Canada). The brightness, contrast, color saturation, and color

temperature of the representative images shown in Figures 1, 2, and 4 were adjusted in Microsoft Powerpoint in order to normalize the background coloring and brightness.

Statistical analysis

Data are expressed as the mean ± SEM unless otherwise indicated. Statistical analyses were carried out using Prism (GraphPad Software, Inc., La Jolla, CA, USA). Prior to analyses, data to be tested were confirmed to be of a normal distribution and F-tests were performed to compare variances between groups. In most instances, the unpaired, two-tailed Student's t test was used to determine significance between an experimental group and a control group with a value of $p \leq 0.05$ considered significant. For comparisons across multiple groups, one-way ANOVA was used. To evaluate differences in effect size between groups, Cohen's delta (Δ) was calculated using mean data for $n = 3$ mice, with a value of $\Delta \geq 0.5$ considered moderate and $\Delta \geq 0.8$ considered a large effect size.

Results

Targeted radiotherapy directs amph-CpG to tumors and improves therapeutic efficacy

To track the delivery of amph-CpG to tumors following radiotherapy, we utilized an image-guided X-irradiator to deliver precise doses of ionizing radiation (IR) to transplanted TUBO mammary carcinoma tumors grown in BALB/c female mice by subcutaneous injection into the hindlimb. TUBO is a cell line derived from a spontaneous tumor formed in a BALB-NeuT transgenic mouse expressing MMTV-rat HER2/Neu [33]. TUBO tumors in BALB/c mice have been used extensively as a model for anti-tumor immunity, including studies where CpG ODNs are provided along with rat HER2-directed vaccines [37, 38]. Here, we examined the distribution of amph-CpG [19], a CpG ODN modified by a 3′ TAMRA ($\lambda_{max}^{ex/em}$ 555/580) or ROX ($\lambda_{max}^{ex/em}$ 575/602) fluorophore to track delivery and a 5′ diacyl lipid tail that mediates binding to serum albumin (Fig. 1A). Thus, three days after radiotherapy, fluorescent amph-CpG was injected i.v. and distribution was tracked over time. As early as two days after injection, we observed enhanced tumor localization of amph-CpG in irradiated tumors (Fig. 1B,C). Furthermore, in tumors irradiated with 10 Gy prior to injection of amph-CpG, fluorescence was retained in tumors for 14 days. This increase in amph-CpG accumulation and retention following radiation-enhanced delivery corresponded to a significant tumor growth delay compared to either treatment on its own (Fig. 1D). Animals treated with amph-CpG displayed no ill effects or weight loss (Supp. Fig. 1).

Augmented tumor delivery of amph-CpG coincides with reduced off-target tissue accumulation

To examine off-target delivery of amph-CpG, tumors and visceral organs were examined *ex vivo* by IVIS fluorescence imaging 24 hrs after injection. Tumors were sliced into sections to compensate for the limited depth of imaging of the IVIS and the radiant efficiencies of those sections were averaged. Irrespective of irradiation, amph-CpG uptake by the spleen, lung and heart was less than that of tumors while accumulation in the liver and kidneys exceeded that of tumors (Fig. 2A,B). While irradiation augmented delivery to tumors, uptake into visceral organs was decreased.

Systemic treatment with CpG ODN can induce splenomegaly through increasing the formation of granulocyte-macrophage colony forming units and early erythroid progenitors in the spleen [39]. Amph-CpG also induced splenomegaly 48 hrs after administration irrespective of tumor irradiation (Fig. 2C). Nonetheless, accumulation of amph-CpG in the spleen at 48 hrs following injection was decreased after tumor irradiation (Fig. 2D).

Activated circulating CD8$^+$ T cells and monocytes induced by combination therapy

To assess the immunological impacts of treatment, peripheral blood was obtained 24 hrs following amph-CpG injection and the mononuclear cells were examined by flow cytometry. While total percentage of various immune cell populations examined were not significantly different from controls (Supp. Fig. 2) in mice treated with both amph-CpG and IR, both CD8$^+$ cytotoxic T lymphocytes and monocytes displayed increased reactive oxygen species (ROS) consistent with activation (Fig. 3A,B). Analysis of the percentage of cells exhibiting a ROS-HI intensity signal revealed a statistically significant increase in effect size induced by combined treatment with amph-CpG and IR as compared to controls (Fig. 3C,D).

Macrophage recruitment and CD8$^+$ T cell immune activity in the tumor after combination treatment

Immunohistochemistry (IHC) of TUBO tumors 48 hrs after amph-CpG treatment revealed an increase in F4/80$^+$ resident macrophages following combination therapy (Fig. 4A) similar to the observed increase in circulating monocytes one day earlier. Increased immunoreactivity for Granzyme B, an enzyme expressed by cytotoxic T lymphocytes and NK cells to mediate target cell death, was also observed in tumors after radiation-enhanced delivery of amph-CpG (Fig. 4B). CpG activates NK cells, and to a lesser extent CD4$^+$ Th1 and CD8$^+$ T lymphocytes, to produce the cytokine IFNγ [7, 40], stimulating B lymphocyte and macrophage activation [41, 42]. Radiation-enhanced amph-CpG delivery appeared to stimulate IFNγ production by immune cells in the tumor by 48 hrs after treatment (Fig. 4C).

Discussion

Both CpG ODN and radiation have long been studied for their potential to promote an anti-tumor immune response. Radiation is thought to serve as an *in situ* vaccine via damaging tumor cells, leading to the release of neoantigens that may be taken up by immature DCs [43, 44]. Although irradiated cells may express damage associated molecular patterns, radiotherapy typically induces very limited anti-tumor immune responses on its own. Synergy between CpG ODN and ionizing radiation in promoting anti-tumor immune response is well described in preclinical models. Acting as an immune adjuvant, CpG ODN binding to TLR9 may drive DC maturation and antigen presentation, resulting in greater CD8$^+$ T cell priming and activation [10–12].

While CpG ODN also appears well suited to potentiate the benefits of radiotherapy in patients, its use has been limited by the low efficacy and high adverse effects associated with systemic administration. Local therapy via intra- or peri-tumoral injection of CpG ODN increases the therapeutic index, both by enhancing colocalization of adjuvant and tumor antigens but also decreasing off-target toxicities. Indeed, intratumoral injection of CpG in

combination with radiotherapy has yielded promising results in clinical trials [45, 46], but may have limited applications.

The studies reported here were designed to take advantage of a distinct mechanism of potential synergy with radiation, based on applying image-guided radiation to target delivery of CpG ODN to tumors. Building on prior work on radiation-induced vascular permeability [47, 48], we recently observed that a single dose of radiation is sufficient to enhance the local extravasation and penetration of circulating macromolecules and nanoparticles, yielding enhanced therapeutic effects of a model nanomedicine [30]. Our prior work established a threshold dose of roughly 5 Gy and demonstrated that radiation's effects were delayed, with optimal delivery when agents were injected three days after irradiation. We also took advantage of the ability of CpG ODN conjugated to a diacyl lipid tail, amph-CpG, to bind serum albumin, thereby increasing circulation time along with providing a means to benefit from the radiation-enhanced permeability effect.

Consistent with the prior studies, we observed that 10 Gy irradiation was sufficient to enhance tumor delivery of amph-CpG injected i.v. three days later. Interestingly, we also observed decreased off-target accumulation in visceral organs, suggesting that the augmented tumor delivery may deplete circulating amph-CpG. The higher levels of intratumoral CpG were associated with increased inflammation with activated macrophages and cytotoxic T cells. A compound effect was observed, leading to greater tumor control than radiation or amph-CpG on their own.

Pre-clinical studies in primates as well as clinical trials conducted in humans revealed that CpG ODN is relatively well tolerated, even with up to weekly dosing for over one year [49–51]. Adverse events associated with CpG treatment that could be avoided with improved delivery via i.v. injection include erythema, pain, swelling, induration, and pruritus at the site of subcutaneous administration [2]. Furthermore, systemic immune activation, including specifically increases in activated $CD8^+$ T cells [52] and activated circulating monocytes [53], has been tied to effective outcomes from cancer immunotherapy. Though past clinical trials have failed due to a lack of antitumor efficacy, CpG ODN remains a promising candidate for combinations with other immunotherapies. For example, CpG increases the cytotoxic antitumor activity of monoclonal antibody (mAb) therapy in mice, even curing large tumors with repeated co-treatments [54, 55]. We anticipate that combining radiation targeting and systemic treatment with amph-CpG may enable broader use and enable new combinations, such as with the emerging immune checkpoint blockade agents.

Supplementary Material

Refer to Web version on PubMed Central for supplementary material.

Acknowledgments

We acknowledge the staff of the Human Tissue Resource Center for tissue processing and embedding. We would also like to thank Dr. Dengping Yin and the Animal Microsurgery Center for their assistance.

Financial support

This work was supported by the NCI via R01s CA164492 and CA199663, by the University of Chicago Cancer Center Support Grant P30CA014599, and by the University of Chicago Ludwig Center for Metastasis Research.

References

1. Klinman DM. Immunotherapeutic uses of CpG oligodeoxynucleotides. Nat Rev Immunol. 2004; 4:249–258. [PubMed: 15057783]
2. Krieg AM. Therapeutic potential of Toll-like receptor 9 activation. Nat Rev Drug Discov. 2006; 5:471–484. [PubMed: 16763660]
3. Hemmi H, Takeuchi O, Kawai T, Kaisho T, Sato S, Sanjo H, Matsumoto M, Hoshino K, Wagner H, Takeda K, Akira S. A Toll-like receptor recognizes bacterial DNA. Nature. 2000; 408:740–745. [PubMed: 11130078]
4. Krieg AM. Antitumor applications of stimulating toll-like receptor 9 with CpG oligodeoxynucleotides. Curr Oncol Rep. 2004; 6:88–95. [PubMed: 14751085]
5. Hacker H, Vabulas RM, Takeuchi O, Hoshino K, Akira S, Wagner H. Immune cell activation by bacterial CpG-DNA through myeloid differentiation marker 88 and tumor necrosis factor receptor-associated factor (TRAF)6. J Exp Med. 2000; 192:595–600. [PubMed: 10952730]
6. Aderem A, Ulevitch RJ. Toll-like receptors in the induction of the innate immune response. Nature. 2000; 406:782–787. [PubMed: 10963608]
7. Klinman DM, Yi AK, Beaucage SL, Conover J, Krieg AM. CpG motifs present in bacteria DNA rapidly induce lymphocytes to secrete interleukin 6, interleukin 12, and interferon gamma. Proc Natl Acad Sci U S A. 1996; 93:2879–2883. [PubMed: 8610135]
8. Ballas ZK, Rasmussen WL, Krieg AM. Induction of NK activity in murine and human cells by CpG motifs in oligodeoxynucleotides and bacterial DNA. J Immunol. 1996; 157:1840–1845. [PubMed: 8757300]
9. Halpern MD, Kurlander RJ, Pisetsky DS. Bacterial DNA induces murine interferon-gamma production by stimulation of interleukin-12 and tumor necrosis factor-alpha. Cell Immunol. 1996; 167:72–78. [PubMed: 8548847]
10. Sparwasser T, Koch ES, Vabulas RM, Heeg K, Lipford GB, Ellwart JW, Wagner H. Bacterial DNA and immunostimulatory CpG oligonucleotides trigger maturation and activation of murine dendritic cells. Eur J Immunol. 1998; 28:2045–2054. [PubMed: 9645386]
11. Jakob T, Walker PS, Krieg AM, Udey MC, Vogel JC. Activation of cutaneous dendritic cells by CpG-containing oligodeoxynucleotides: a role for dendritic cells in the augmentation of Th1 responses by immunostimulatory DNA. J Immunol. 1998; 161:3042–3049. [PubMed: 9743369]
12. Hartmann G, Weiner GJ, Krieg AM. CpG DNA: a potent signal for growth, activation, and maturation of human dendritic cells. Proc Natl Acad Sci U S A. 1999; 96:9305–9310. [PubMed: 10430938]
13. Stacey KJ, Sweet MJ, Hume DA. Macrophages ingest and are activated by bacterial DNA. J Immunol. 1996; 157:2116–2122. [PubMed: 8757335]
14. Roman M, Martin-Orozco E, Goodman JS, Nguyen MD, Sato Y, Ronaghy A, Kornbluth RS, Richman DD, Carson DA, Raz E. Immunostimulatory DNA sequences function as T helper-1-promoting adjuvants. Nat Med. 1997; 3:849–854. [PubMed: 9256274]
15. Carpentier AF, Chen L, Maltonti F, Delattre JY. Oligodeoxynucleotides containing CpG motifs can induce rejection of a neuroblastoma in mice. Cancer Res. 1999; 59:5429–5432. [PubMed: 10554011]
16. Kawarada Y, Ganss R, Garbi N, Sacher T, Arnold B, Hammerling GJ. NK− and CD8(+) T cell-mediated eradication of established tumors by peritumoral injection of CpG-containing oligodeoxynucleotides. J Immunol. 2001; 167:5247–5253. [PubMed: 11673539]
17. Heckelsmiller K, Rall K, Beck S, Schlamp A, Seiderer J, Jahrsdorfer B, Krug A, Rothenfusser S, Endres S, Hartmann G. Peritumoral CpG DNA elicits a coordinated response of CD8 T cells and innate effectors to cure established tumors in a murine colon carcinoma model. J Immunol. 2002; 169:3892–3899. [PubMed: 12244187]

18. Lou Y, Liu C, Lizee G, Peng W, Xu C, Ye Y, Rabinovich BA, Hailemichael Y, Gelbard A, Zhou D, Overwijk WW, Hwu P. Antitumor activity mediated by CpG: the route of administration is critical. J Immunother. 2011; 34:279–288. [PubMed: 21389870]
19. Liu H, Moynihan KD, Zheng Y, Szeto GL, Li AV, Huang B, Van Egeren DS, Park C, Irvine DJ. Structure-based programming of lymph-node targeting in molecular vaccines. Nature. 2014; 507:519–522. [PubMed: 24531764]
20. Sleep D, Cameron J, Evans LR. Albumin as a versatile platform for drug half-life extension. Biochim Biophys Acta. 2013; 1830:5526–5534. [PubMed: 23639804]
21. Baines J, Celis E. Immune-mediated tumor regression induced by CpG-containing oligodeoxynucleotides. Clin Cancer Res. 2003; 9:2693–2700. [PubMed: 12855649]
22. Blazar BR, Krieg AM, Taylor PA. Synthetic unmethylated cytosine-phosphate-guanosine oligodeoxynucleotides are potent stimulators of antileukemia responses in naive and bone marrow transplant recipients. Blood. 2001; 98:1217–1225. [PubMed: 11493473]
23. Ballas ZK, Krieg AM, Warren T, Rasmussen W, Davis HL, Waldschmidt M, Weiner GJ. Divergent therapeutic and immunologic effects of oligodeoxynucleotides with distinct CpG motifs. J Immunol. 2001; 167:4878–4886. [PubMed: 11673492]
24. CS Nicklin PS, Phillips JA. Pharmacokinetic properties of phosphorothioates in animals—absorption, distribution, metabolism and elimination, in: S. Crooke (Ed.). Antisense Research and Application, Springer, Berlin. 1998:141–168.
25. Maeda H, Nakamura H, Fang J. The EPR effect for macromolecular drug delivery to solid tumors: Improvement of tumor uptake, lowering of systemic toxicity, and distinct tumor imaging in vivo. Adv Drug Deliv Rev. 2013; 65:71–79. [PubMed: 23088862]
26. Prabhakar U, Maeda H, Jain RK, Sevick-Muraca EM, Zamboni W, Farokhzad OC, Barry ST, Gabizon A, Grodzinski P, Blakey DC. Challenges and key considerations of the enhanced permeability and retention effect for nanomedicine drug delivery in oncology. Cancer Res. 2013; 73:2412–2417. [PubMed: 23423979]
27. Suzuki Y, Wakita D, Chamoto K, Narita Y, Tsuji T, Takeshima T, Gyobu H, Kawarada Y, Kondo S, Akira S, Katoh H, Ikeda H, Nishimura T. Liposome-encapsulated CpG oligodeoxynucleotides as a potent adjuvant for inducing type 1 innate immunity. Cancer Res. 2004; 64:8754–8760. [PubMed: 15574787]
28. Zhang XQ, Dahle CE, Baman NK, Rich N, Weiner GJ, Salem AK. Potent antigen-specific immune responses stimulated by codelivery of CpG ODN and antigens in degradable microparticles. J Immunother. 2007; 30:469–478. [PubMed: 17589287]
29. Borges O, Tavares J, Sousa A de, Borchard G, Junginger HE, Cordeiro-da-Silva A. Evaluation of the immune response following a short oral vaccination schedule with hepatitis B antigen encapsulated into alginate-coated chitosan nanoparticles. Eur J Pharm Sci. 2007; 32:278–290. [PubMed: 17884394]
30. Appelbe OK, Zhang Q, Pelizzari CA, Weichselbaum RR, Kron SJ. Image-Guided Radiotherapy Targets Macromolecules through Altering the Tumor Microenvironment. Mol Pharm. 2016
31. Mount D, Bruce WR. Local Plasma Volume and Vascular Permeability of Rabbit Skin after Irradiation. Radiat Res. 1964; 23:430–445. [PubMed: 14223315]
32. Law MP, Thomlinson RH. Vascular permeability in the ears of rats after x-irradiation. Br J Radiol. 1978; 51:895–904. [PubMed: 709038]
33. Boggio K, Nicoletti G, Di Carlo E, Cavallo F, Landuzzi L, Melani C, Giovarelli M, Rossi I, Nanni P, De Giovanni C, Bouchard P, Wolf S, Modesti A, Musiani P, Lollini PL, Colombo MP, Forni G. Interleukin 12-mediated prevention of spontaneous mammary adenocarcinomas in two lines of Her-2/neu transgenic mice. J Exp Med. 1998; 188:589–596. [PubMed: 9687535]
34. Moding EJ, Clark DP, Qi Y, Li Y, Ma Y, Ghaghada K, Johnson GA, Kirsch DG, Badea CT. Dual-energy micro-computed tomography imaging of radiation-induced vascular changes in primary mouse sarcomas. Int J Radiat Oncol Biol Phys. 2013; 85:1353–1359. [PubMed: 23122984]
35. CM, Ma, Coffey, CW., DeWerd, LA., Liu, C., Nath, R., Seltzer, SM., Seuntjens, JP., M. American Association of Physicists. AAPM protocol for 40–300 kV x-ray beam dosimetry in radiotherapy and radiobiology. Med Phys. 2001; 28:868–893. [PubMed: 11439485]

36. Inoue Y, Izawa K, Kiryu S, Tojo A, Ohtomo K. Diet and abdominal autofluorescence detected by in vivo fluorescence imaging of living mice. Mol Imaging. 2008; 7:21–27. [PubMed: 18384720]
37. Sharma S, Dominguez AL, Manrique SZ, Cavallo F, Sakaguchi S, Lustgarten J. Systemic targeting of CpG-ODN to the tumor microenvironment with anti-neu-CpG hybrid molecule and T regulatory cell depletion induces memory responses in BALB-neuT tolerant mice. Cancer Res. 2008; 68:7530–7540. [PubMed: 18794141]
38. Nava-Parada P, Forni G, Knutson KL, Pease LR, Celis E. Peptide vaccine given with a Toll-like receptor agonist is effective for the treatment and prevention of spontaneous breast tumors. Cancer Res. 2007; 67:1326–1334. [PubMed: 17283170]
39. Sparwasser T, Hultner L, Koch ES, Luz A, Lipford GB, Wagner H. Immunostimulatory CpG-oligodeoxynucleotides cause extramedullary murine hemopoiesis. J Immunol. 1999; 162:2368–2374. [PubMed: 9973517]
40. Cowdery JS, Chace JH, Yi AK, Krieg AM. Bacterial DNA induces NK cells to produce IFN-gamma in vivo and increases the toxicity of lipopolysaccharides. J Immunol. 1996; 156:4570–4575. [PubMed: 8648098]
41. Murray HW. Interferon-gamma, the activated macrophage, and host defense against microbial challenge. Ann Intern Med. 1988; 108:595–608. [PubMed: 3126690]
42. Yi AK, Chace JH, Cowdery JS, Krieg AM. IFN-gamma promotes IL-6 and IgM secretion in response to CpG motifs in bacterial DNA and oligodeoxynucleotides. J Immunol. 1996; 156:558–564. [PubMed: 8543806]
43. Mason KA, Ariga H, Neal R, Valdecanas D, Hunter N, Krieg AM, Whisnant JK, Milas L. Targeting toll-like receptor 9 with CpG oligodeoxynucleotides enhances tumor response to fractionated radiotherapy. Clin Cancer Res. 2005; 11:361–369. [PubMed: 15671567]
44. Reits EA, Hodge JW, Herberts CA, Groothuis TA, Chakraborty M, Wansley EK, Camphausen K, Luiten RM, de Ru AH, Neijssen J, Griekspoor A, Mesman E, Verreck FA, Spits H, Schlom J, van Veelen P, Neefjes JJ. Radiation modulates the peptide repertoire, enhances MHC class I expression, and induces successful antitumor immunotherapy. J Exp Med. 2006; 203:1259–1271. [PubMed: 16636135]
45. Brody JD, Ai WZ, Czerwinski DK, Torchia JA, Levy M, Advani RH, Kim YH, Hoppe RT, Knox SJ, Shin LK, Wapnir I, Tibshirani RJ, Levy R. In situ vaccination with a TLR9 agonist induces systemic lymphoma regression: a phase I/II study. J Clin Oncol. 2010; 28:4324–4332. [PubMed: 20697067]
46. Kim YH, Gratzinger D, Harrison C, Brody JD, Czerwinski DK, Ai WZ, Morales A, Abdulla F, Xing L, Navi D, Tibshirani RJ, Advani RH, Lingala B, Shah S, Hoppe RT, Levy R. In situ vaccination against mycosis fungoides by intratumoral injection of a TLR9 agonist combined with radiation: a phase 1/2 study. Blood. 2012; 119:355–363. [PubMed: 22045986]
47. Baumann BC, Kao GD, Mahmud A, Harada T, Swift J, Chapman C, Xu X, Discher DE, Dorsey JF. Enhancing the efficacy of drug-loaded nanocarriers against brain tumors by targeted radiation therapy. Oncotarget. 2013; 4:64–79. [PubMed: 23296073]
48. Giustini AJ, Petryk AA, Hoopes PJ. Ionizing radiation increases systemic nanoparticle tumor accumulation. Nanomedicine. 2012; 8:818–821. [PubMed: 22633900]
49. Davis HL, Suparto II, Weeratna RR, Jumintarto, Iskandriati DD, Chamzah SS, Ma'ruf AA, Nente CC, Pawitri DD, Krieg, Heriyanto A, Smits W, Sajuthi DD. CpG DNA overcomes hyporesponsiveness to hepatitis B vaccine in orangutans. Vaccine. 2000; 18:1920–1924. [PubMed: 10699341]
50. Jones TR, Obaldia N 3rd, Gramzinski RA, Charoenvit Y, Kolodny N, Kitov S, Davis HL, Krieg AM, Hoffman SL. Synthetic oligodeoxynucleotides containing CpG motifs enhance immunogenicity of a peptide malaria vaccine in Aotus monkeys. Vaccine. 1999; 17:3065–3071. [PubMed: 10462241]
51. Krieg A, Efler S, Price J, Al-Adhami M, Whisnant J. Biomarker profile and clinical safety of SC or IV doses of Promune (TM)(CpG 7909 injection) a novel TLR-9 agonist Oligodeoxynucleotide, in. Journal of Immunotherapy, LIPPINCOTT WILLIAMS & WILKINS 530 WALNUT ST, PHILADELPHIA, PA 19106-3621 USA. 2003:S34–S34.

52. Yang SX, Wei WS, Ouyan QW, Jiang QH, Zou YF, Qu W, Tu JH, Zhou ZB, Ding HL, Xie CW, Lei QM, Zhong CR. Interleukin-12 activated CD8+ T cells induces apoptosis in breast cancer cells and reduces tumor growth. Biomed Pharmacother. 2016; 84:1466–1471. [PubMed: 27810342]

53. Spitzer MH, Carmi Y, Reticker-Flynn NE, Kwek SS, Madhireddy D, Martins MM, Gherardini PF, Prestwood TR, Chabon J, Bendall SC, Fong L, Nolan GP, Engleman EG. Systemic Immunity Is Required for Effective Cancer Immunotherapy. Cell. 2017; 168:487–502e415. [PubMed: 28111070]

54. Wooldridge JE, Ballas Z, Krieg AM, Weiner GJ. Immunostimulatory oligodeoxynucleotides containing CpG motifs enhance the efficacy of monoclonal antibody therapy of lymphoma. Blood. 1997; 89:2994–2998. [PubMed: 9108420]

55. Warren TL, Dahle CE, Weiner GJ. CpG oligodeoxynucleotides enhance monoclonal antibody therapy of a murine lymphoma. Clin Lymphoma. 2000; 1:57–61. [PubMed: 11707814]

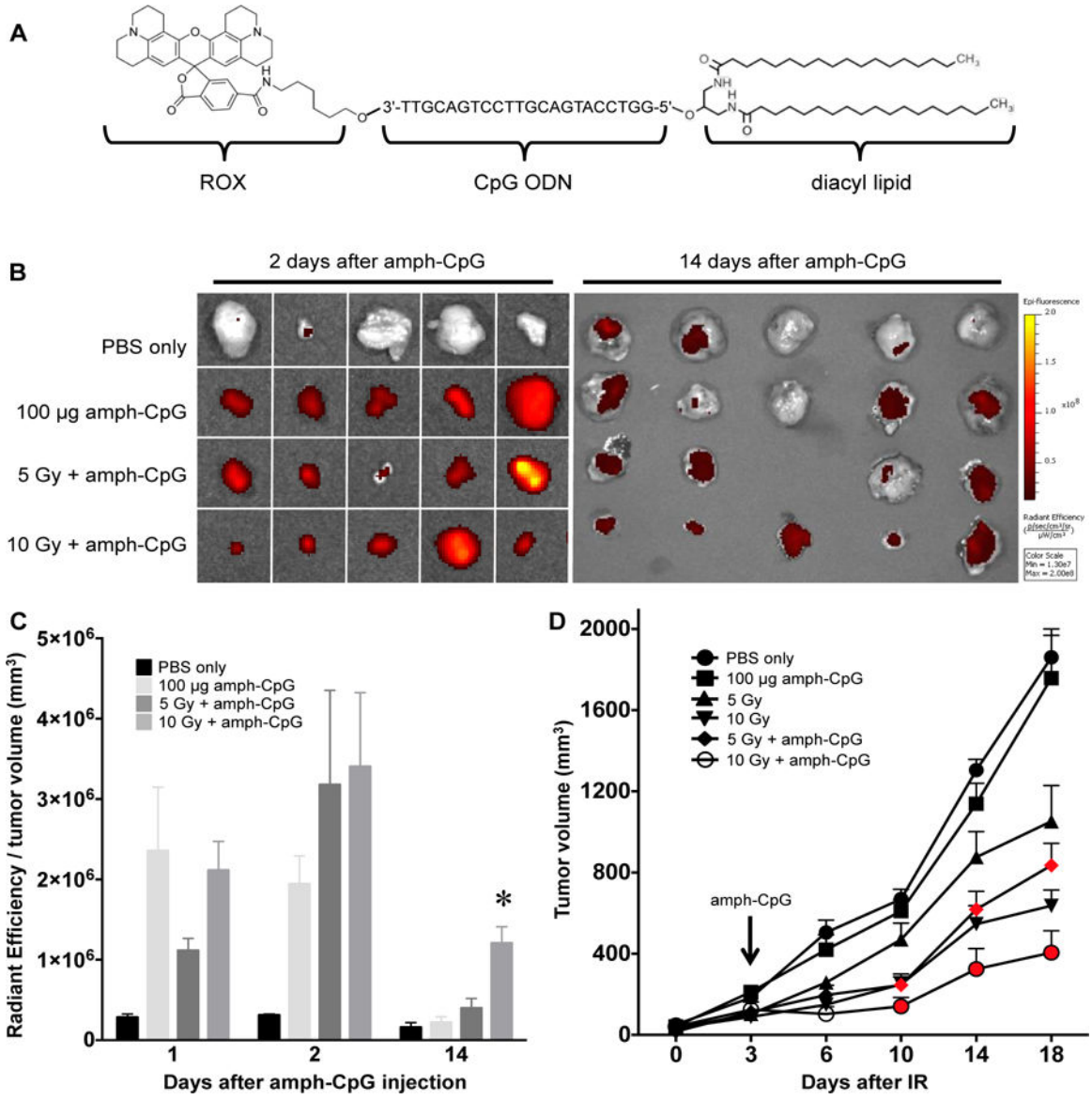

Figure 1.

Radiation-enhanced delivery of amph-CpG increases anti-tumor effectiveness. A) CpG ODN conjugated to a 5′ diacyl lipid tail and a 3′ ROX dye to create fluorescent amph-CpG. B) Targeted radiotherapy increases the tumor accumulation of systemically administered amph-CpG, as observed through IVIS fluorescence imaging (black to yellow gradient). C) IVIS quantification of tumor fluorescence measured at multiple time points shows significantly increased accumulation and retention of amph-CpG in irradiated tumors. n = 3–5 for each data set; * $p \leq 0.05$. D) Tumor growth significantly decreases over time following IR + amph-CpG treatment. Red denotes time points where combination treatment significantly decreased tumor size relative to IR alone. n = 5–9 for each data set; $p \leq 0.05$.

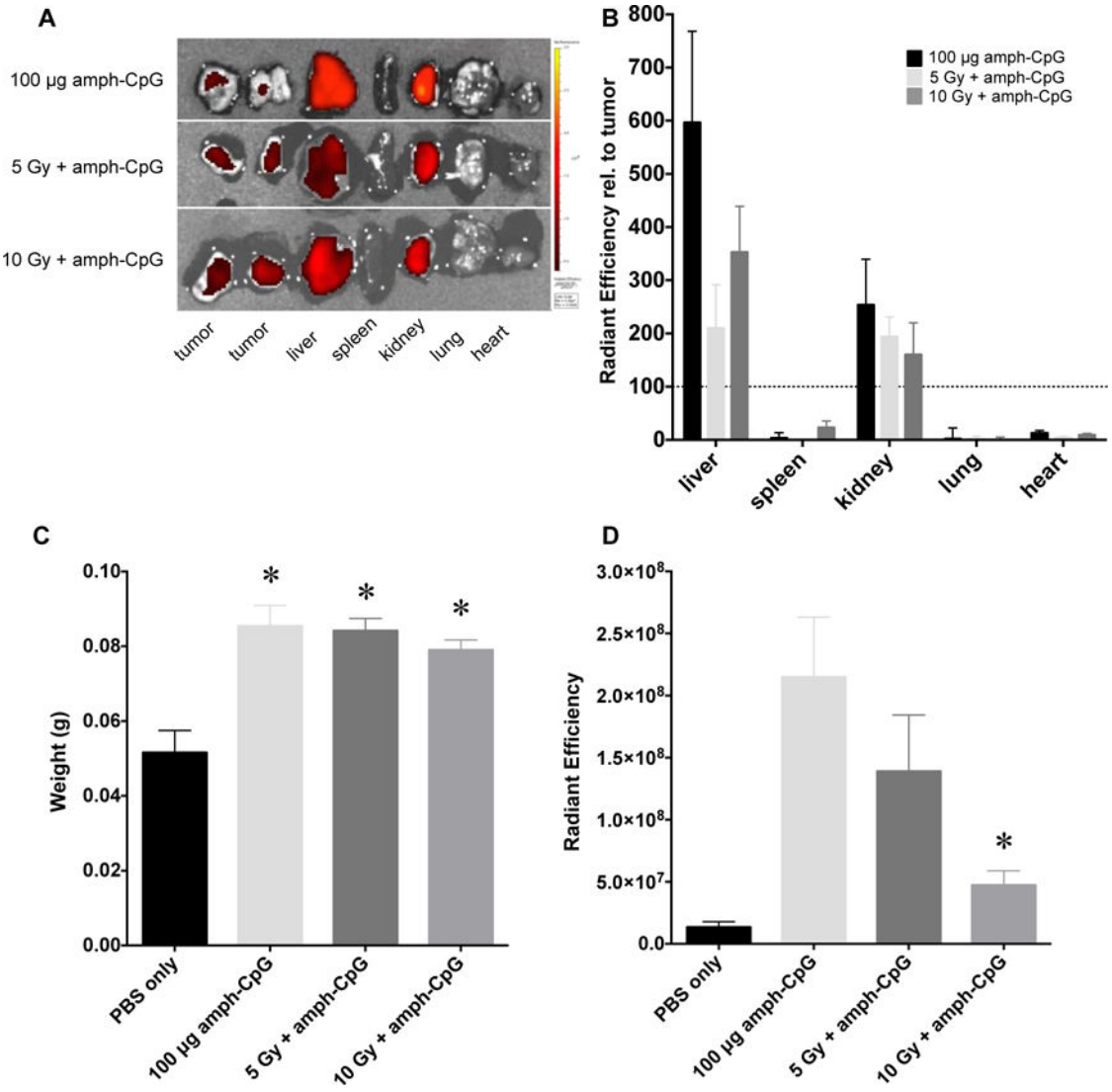

Figure 2.

Using radiation to target tumor-specific delivery of amph-CpG decreases off-target tissue accumulation. A) IVIS imaging of amph-CpG fluorescence in multiple vital tissues 24 hrs after administration (black to yellow gradient). Representative images shown. B) IVIS quantification of off-target tissue amph-CpG accumulation 24 hrs after administration, relative to tumor accumulation (dotted line). n = 3 for each data set. C) Spleen weight 48 hrs after amph-CpG administration. n = 5 for each data set; * $p \leq 0.05$ relative to PBS only control. D) IVIS quantification of spleen amph-CpG uptake 48 hrs after administration. n = 5 for each data set; * $p \leq 0.05$ relative to amph-CpG only.

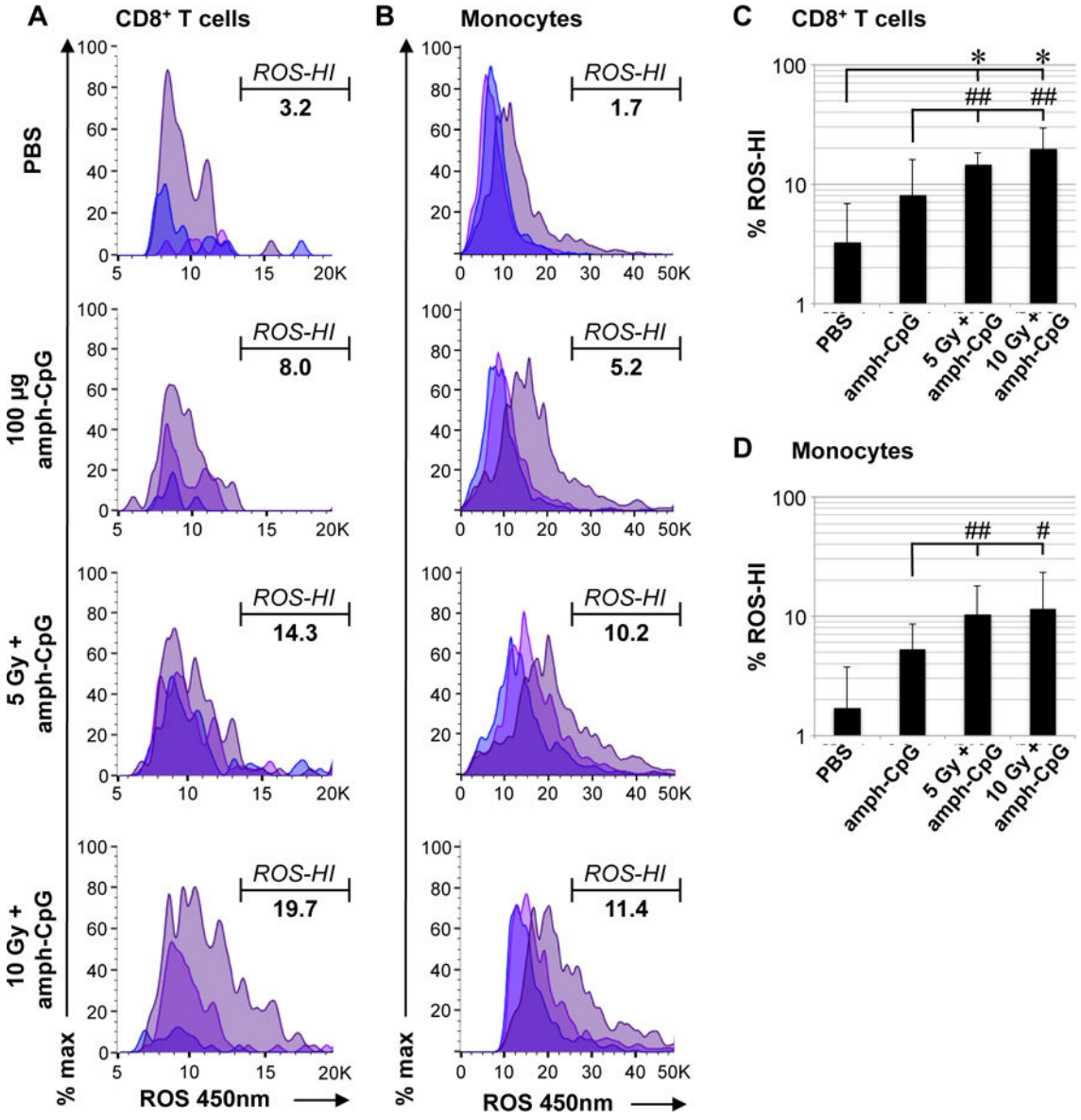

Figure 3.

Irradiation enhances amph-CpG activation of cytotoxic T lymphocytes and monocytes in circulating blood as measured by reactive oxygen species (ROS) generation. A) ROS staining indicating activation of $CD8^+$ T cells by IR + amph-CpG treatment. Populations shown: viable single $CD8^+$ T cells from each of three mice per condition, histograms overlaid. Percentage indicates mean % ROS-HI cells. B) ROS staining shows activation of circulating monocytes by IR + amph-CpG treatment. Populations shown: viable single monocytes from each of three mice per condition, histograms overlaid. Percentage indicates mean % ROS-HI cells. C) Data summary for percentage of ROS-HI circulating $CD8^+$ T cells. D) Data summary for percentage of ROS-HI circulating monocytes. * indicates significance (two-sided, unpaired t-test $p \leq 0.05$), # indicates effect size (Cohen's delta $\Delta \geq 0.5$, ## indicates $\Delta \geq 0.8$), error bar = 1 S.D. for n = 3 mice.

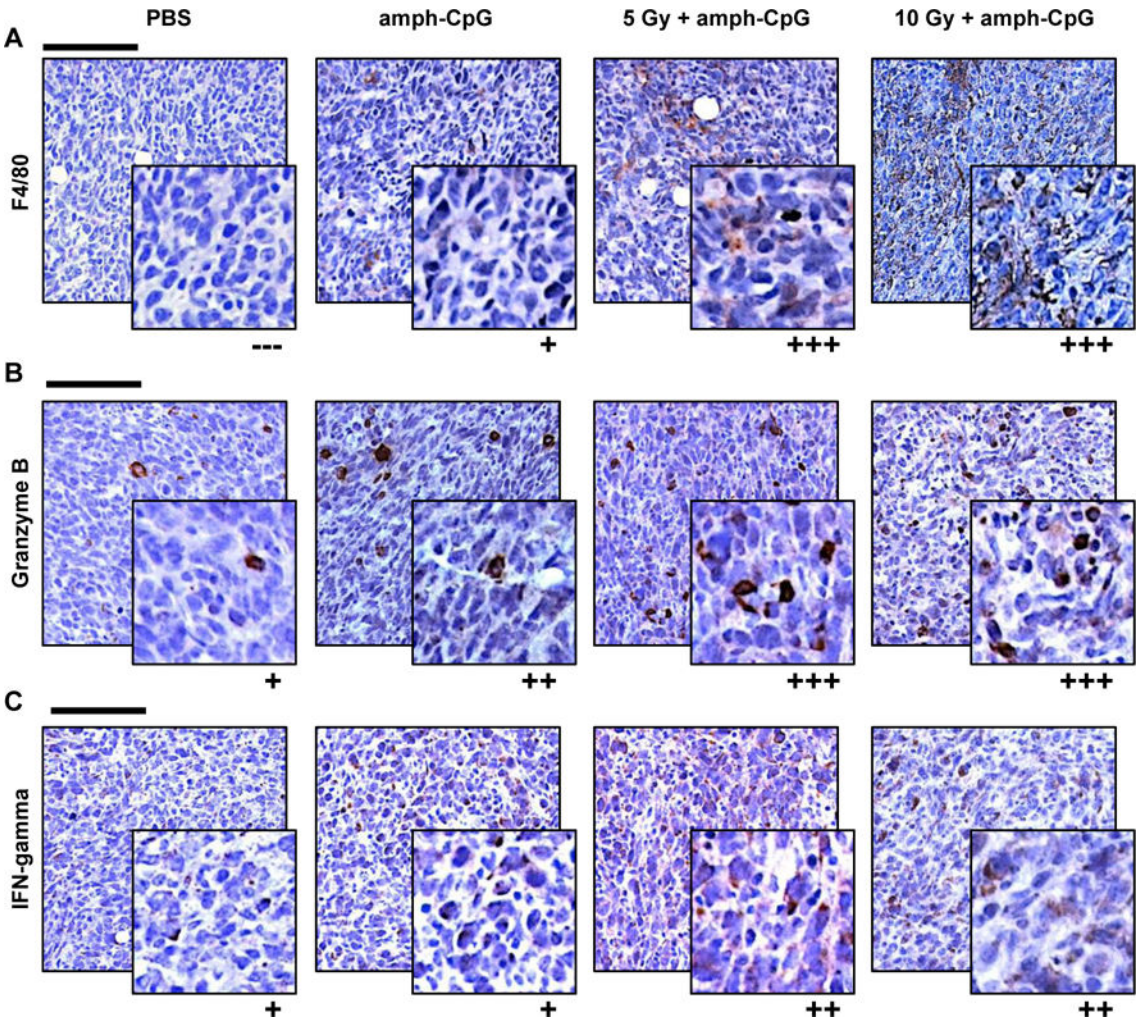

Figure 4.

Up-regulation of immune activity evident within TUBO tumors 48 hrs following radiation-enhanced delivery of amph-CpG. A) The increase in circulating monocytes seen after radiation-enhanced delivery coincided with an observed macrophage increase in tumor sections by IHC (brown = F4/80, macrophages). B) $CD8^+$ T lymphocytes in tumor sections displayed increased Granzyme B immunoreactivity (brown) after IR. C) NK cell activity (brown = IFNγ) appeared up-regulated in tumor sections following IR + amph-CpG. In all IHC images, purple = hematoxylin, nuclei. Scale bar = 100 μm. Inset = 4X zoom. Qualitative scoring: (−−−) negative, (+) faint staining of some cells, (++) moderate staining of many cells, (+++) intense staining of many cells. Representative images shown of n = 3 tumors per data set stained.